Neutron excitations in ^{119}Ba

K. K. Zheng,[1,2] C. M. Petrache,[1] Z. H. Zhang,[3] A. Astier,[1] B. F. Lv,[1,*] P. T. Greenlees,[4] T. Grahn,[4] R. Julin,[4] S. Juutinen,[4] M. Luoma,[4] J. Ojala,[4] J. Pakarinen,[4] J. Partanen,[4,†] P. Rahkila,[4] P. Ruotsalainen,[4] M. Sandzelius,[4] J. Sarén,[4] H. Tann,[4,5] J. Uusitalo,[4] G. Zimba,[4] B. Cederwall,[6] Ö. Aktas,[6] A. Ertoprak,[6] W. Zhang,[6] S. Guo,[2,7] M. L. Liu,[2,7] X. H. Zhou,[2,7] I. Kuti,[8] B. M. Nyakó,[8] D. Sohler,[8] J. Timár,[8] C. Andreoiu,[9] M. Doncel,[5] D. T. Joss,[5] and R. D. Page[5]

[1]*Université Paris-Saclay, CNRS/IN2P3, IJCLab, 91405 Orsay, France*

[2]*Key Laboratory of High Precision Nuclear Spectroscopy and Center for Nuclear Matter Science, Institute of Modern Physics, Chinese Academy of Sciences, Lanzhou 730000, People's Republic of China*

[3]*Mathematics and Physics Department, North China Electric Power University, Beijing 102206, China*

[4]*Department of Physics, University of Jyväskylä, P.O. Box 35, FI-40014, University of Jyväskylä, Finland*

[5]*Oliver Lodge Laboratory, Department of Physics, University of Liverpool, Liverpool L69 7ZE, United Kingdom*

[6]*KTH Department of Physics, S-10691 Stockholm, Sweden*

[7]*School of Nuclear Science and Technology, University of Chinese Academy of Science, Beijing 100049, People's Republic of China*

[8]*Institute for Nuclear Research (ATOMKI), 4001 Debrecen, Hungary*

[9]*Department of Chemistry, Simon Fraser University, Burnaby, BC V5A 1S6, Canada*

(Received 19 April 2021; accepted 22 July 2021; published 30 July 2021)

The neutron-deficient ^{119}Ba nucleus has been studied using the ^{58}Ni(^{64}Zn, $2pn$) reaction and the JUROGAM 3 γ-ray detector array coupled to the MARA recoil-mass separator setup. One new rotational band and several low-lying states are newly identified. A half-life of $T_{1/2} = 0.36(2)$ μs has been measured for the $5/2^-$ bandhead of the $\nu h_{11/2}$ band. The two previously known rotational bands are confirmed, except for the higher part of the $+1/2$ signature partner of the positive-parity band. Configurations are assigned based on the analysis of the observed quasiparticle alignments whose nature is unveiled by the calculations using the particle number conserving cranked shell model.

DOI: 10.1103/PhysRevC.104.014326

I. INTRODUCTION

The study of the lightest Ba nuclei is confronted with the increasing difficulty to populate high-spin states using fusion-evaporation reactions, due to the limited choice of projectile-target combinations and the small cross sections for the evaporation of neutrons close to the proton drip-line. The existing experimental information on high-spin states in very-proton-rich nuclei is therefore increasingly scarce towards the proton-drip line. The lightest odd-even ^{117,119}Ba nuclei with known rotational bands have been studied using the high-efficiency γ-detector array GAMMASPHERE [1] coupled with the recoil mass separator FMA [2] employing the ^{58}Ni(^{64}Zn, $2pxn$) fusion-evaporation reactions [3,4], while ^{121}Ba has been studied using the γ-detector array NORDBALL consisting of 15 Compton-suppressed Ge detectors and ancillary detectors for neutrons and protons employing the ^{92}Mo(^{32}S, $p2n$) reaction [5]. Two or three rotational bands have been observed in these odd-even Ba nuclei, but no detailed spectroscopy of the low-lying states was performed until now.

The present work is devoted to the study of ^{119}Ba, in which two bands based on opposite-parity orbitals are known [4]. The experimental data were obtained from a high-statistics experiment performed with the γ-detector array JUROGAM 3 [6] coupled with the recoil mass separator MARA [7] employing the ^{58}Ni(^{64}Zn, $2pn$) ^{119}Ba reaction at a beam energy of 255 MeV. Several results on the structure of ^{119}Cs obtained from the same experiment have been recently published or submitted for publication [8–10]. Experimental details have been already included in those articles and therefore are not repeated here.

We report the following experimental results on ^{119}Ba: Identification of a new positive-parity band and of several low-lying states, measurement of a $T_{1/2} = 0.36(2)$ μs half-life of the $5/2^-$ bandhead of the $\nu h_{11/2}$ band, and change of the high-spin part of the known $\alpha = +1/2$ signature partner of the band built on the $\nu g_{7/2}[413]5/2^+$ orbital. We discuss the configurations of the observed bands, which are assigned based on the quasiparticle alignment analysis and on particle number conserving cranked shell-model (PNC-CSM) calculations [11,12].

II. EXPERIMENTAL RESULTS

The complete experimental information on the γ-ray transitions of ^{119}Ba is given in Table I of the Appendix. The level scheme including the previously known and the newly

*Present address: Key Laboratory of High Precision Nuclear Spectroscopy and Center for Nuclear Matter Science, Institute of Modern Physics, Chinese Academy of Sciences, Lanzhou 730000, People's Republic of China.

†Deceased.

observed bands, as well as a zoom on the low-lying levels are shown in Figs. 1 and 2, respectively. Double-gated spectra obtained from prompt $\gamma\gamma\gamma$ coincidences showing the newly identified transitions are shown in Figs. 3 and 4. Spectra for Band 1 obtained from prompt-delayed coincidences of γ rays detected by JUROGAM 3 and the detectors at the MARA focal plane are shown in Fig. 5.

The assignment of the bands to ^{119}Ba is based on the coincidence of the prompt γ-γ coincidences with recoiling evaporation residues with mass 119 detected at the MARA focal plane, and with the 31 keV K_α and 35 keV K_β x-rays of barium nuclides detected in prompt coincidence with the in-band transitions by JUROGAM 3 array at the target position (see, e.g., the spectra of Band 1 in Fig. 5). The bands have been established based on coincidence relationships, intensity balance of the states, and when possible, on the angular correlations of the observed γ rays. We adopt spin-parity $5/2^-$ for the bandhead of the negative-parity band, and $7/2^+$ for the second lowest state of the positive-parity band, in agreement with the previous assignments based on delayed proton emission and on systematics [13].

Band 2 was previously assigned to ^{119}Ba in Ref. [4], in which the states at the bottom of the band were not understood, and the spin-parity of the ground state could not be firmly assigned. However, based on the systematics of the positive-parity bands in odd-even Ba nuclei (see, e.g., Refs. [3,4]), a spin-parity $5/2^+$ was proposed for the state depopulated by the 53-keV transition, which is confirmed by the present work and adopted as bandhead of Band 2. We also report evidence of a new band, which we label Band 3 and which decays via the 92- and 239-keV transitions to the same $3/2^+$ lowest level to which also Bands 1 and 2 decay. The spin and parity $I^\pi = 3/2^+$ of this lowest level fed by all observed bands are fixed by the angular correlations of the four feeding transitions from Bands 2 and 3, which have spins and parities assigned based on systematics and on the existence of several interconnecting transitions. We assign it as the bandhead of Band 3 and the ground state of ^{119}Ba, which is in agreement with the previous assignment [13]. As discussed in the following, the configurations assigned to Bands 2 and 3, $\nu g_{7/2}[413]5/2^+$ and $\nu d_{5/2}[411]3/2^+$, respectively, are also in agreement with the adopted $5/2^+$ and $3/2^+$ bandheads of the two bands. One should note that the measured β-delayed proton spectrum of ^{119}Ba has been qualitatively reproduced in terms of the statistical model in Ref. [14] assuming $I^\pi = 5/2^\pm$ for the ground state, but with a centroid at slightly higher energy than the experimental one. The presently assigned ground state spin-parity $3/2^+$ was not investigated in Ref. [14].

Band 1, previously assigned to ^{119}Ba in Ref. [4], is confirmed up to $55/2^-$. The 1266-keV transition observed in Ref. [4] and placed on the side of Band 1 is now placed on top of the $55/2^-$ state and becomes the highest transition of Band 1 (see Fig. 1). The transitions above the $55/2^-$ state reported in Ref. [4] are not observed in the present data set even though the statistics is sufficient for their observation [see the spectrum shown in Fig. 4(a)]. It was known that the state fed by the 60-keV transition has an isomeric character, because no prompt transitions depopulating it were observed [4]. This state was assigned as the bandhead, and a spin-parity $I^\pi = 5/2^-$ was assigned based on the systematics of the observed bands in odd-even Ba nuclei [4]. We searched for delayed transitions detected at the MARA focal plane in coincidence with the prompt transitions of Band 1 measured at the target position, and succeed in identifying three delayed transitions with energies of 53, 59, and 66 keV, which are not in mutual coincidence and therefore can be placed in parallel below the $5/2^-$ isomer. We could not perform an angular-correlation analysis of the events measured at the MARA focal plane. Therefore, the electromagnetic character of these transitions could not be established experimentally, but only tentatively assigned.

We extracted a half-life of $T_{1/2} = 0.36(2)$ μs from the fit of the time spectrum of the 66-keV transition, which is the strongest of the three delayed transitions (see Fig. 6). Similar half-lives but with larger errors could be extracted from the time spectra of the 53- and 59-keV transitions.

To qualitatively account for the half-life of the $5/2^-$ isomer, we analyzed the Weisskopf estimates of the partial half-lives associated with the depopulation of the $5/2^-$ isomer via the two cascades 7–59 keV, 13–53 keV, and the parallel 66-keV ($5/2^- \rightarrow 3/2^+$) $E1$ transition. By assuming a 10^{-6} hindrance for all $E1$ transitions and no hindrance for the $M1/E2$ transitions, and examining all combinations of multipolarities, parities, and order of the transitions in the two cascades, the closest value to the measured half-life is $T_{1/2} = 0.22(16)$ μs, which is obtained when the 7- and 13-keV transitions have $M1/E2$ and $E1$ characters, and are placed on top of the 59- and 53-keV transitions, respectively. We therefore tentatively assign spin-parity $(3/2^-)$ to the state populated by the 7-keV transition. A 53-keV transition is also known as the lowest transition in Band 2 [4], being observed in prompt coincidence at the target position. We therefore conclude that the 53-keV transitions observed both at the MARA focal plane in delayed coincidence with transitions of Band 1 measured at the target position, and at the target position in prompt coincidence with transitions of Band 2, are in fact the same transition depopulating the $5/2^+$ bandhead of Band 2, which is fed by the prompt 123- and 285-keV transitions of Band 2 and by the delayed 13-keV transition from the isomeric bandhead of Band 1. The $5/2^-$ bandhead of band 1 decays therefore to the $3/2^+$ ground state via the cascade 7–59 keV and the 66-keV transition, as well as to the bandhead of Band 2 via the 13-keV transition.

Seven out-of-band transitions are observed from the states of Band 2 to states of Band 3 and to the new $7/2^+$ state placed in between Bands 2 and 3. The negative-signature partner of Band 2 is confirmed up to spin 75/2 (see Figs. 1 and 4). The previously reported 361- and 364-keV transitions between the signature partner cascades, as well as the highest 1578-keV transition in the negative-signature partner [4], are not observed in the present experiment. The $+1/2$ signature partner of Band 2 is confirmed up to spin 29/2, on top of which two transitions of 740 and 807 keV are placed. The previously reported 796-, 897- and 997-keV transitions in Ref. [4] are not confirmed. The presence of the 796- and 897-keV transitions in the spectra of Ref. [4] may possibly be due to contamination from ^{115}I, a well-populated nucleus

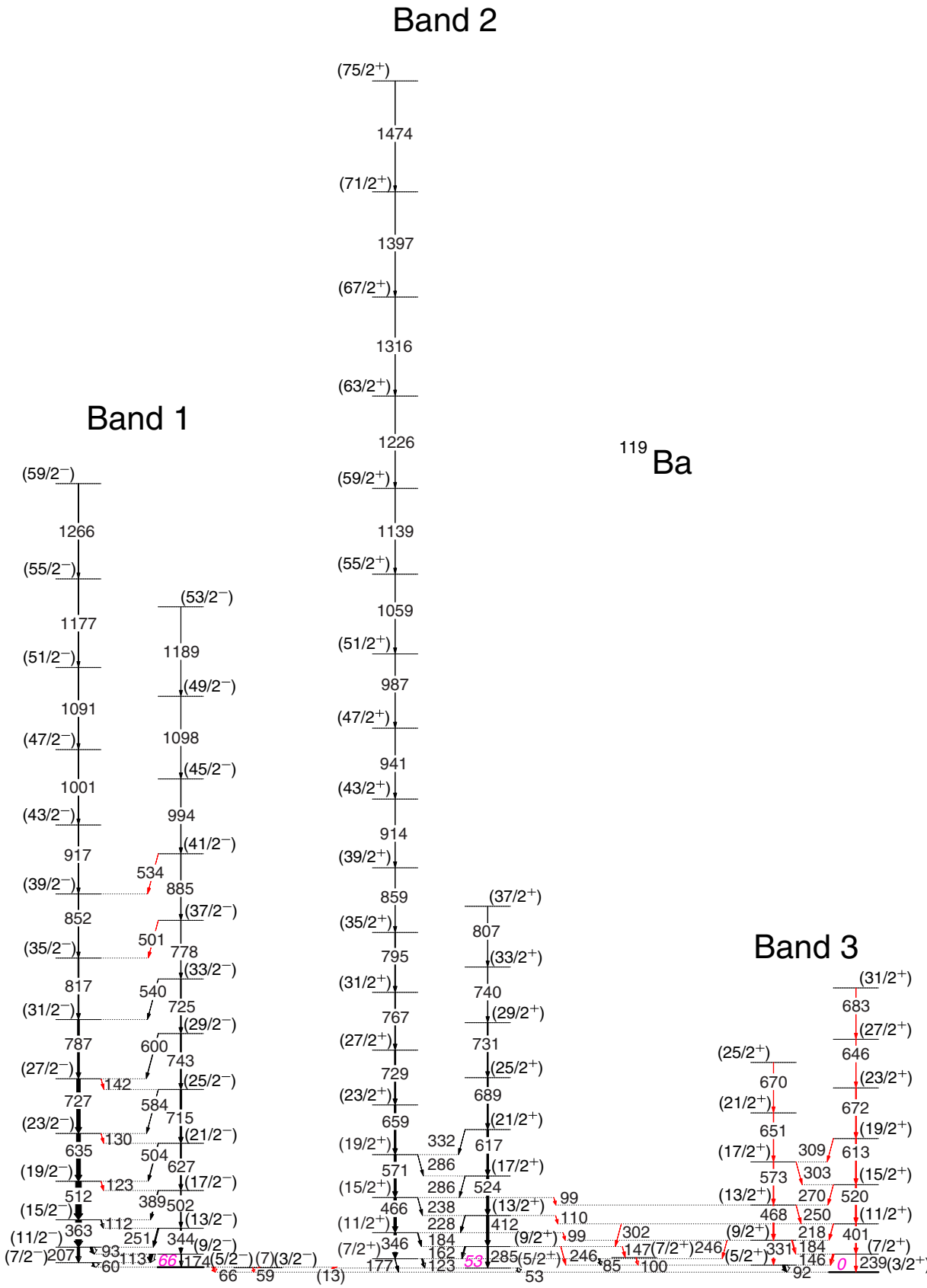

FIG. 1. Level scheme of ^{119}Ba. The new transitions are indicated with red, the bandhead energies of the three bands are indicated in pink, the isomeric and tentative levels are indicated with thick and dashed lines, respectively. The arrow widths are proportional to the transition intensities.

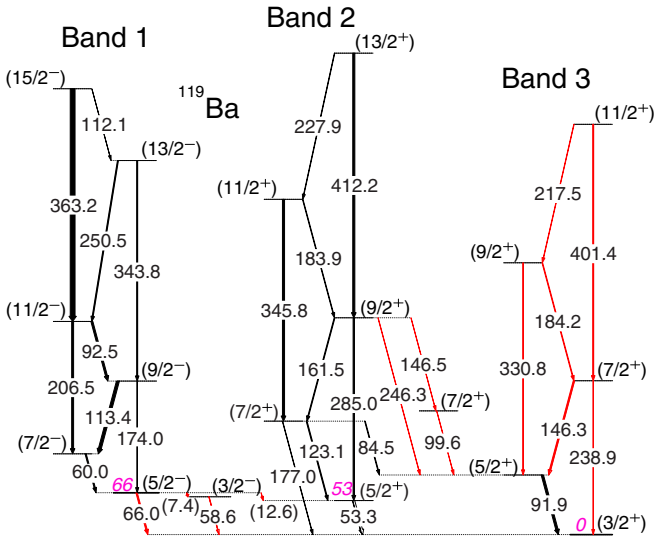

FIG. 2. The same as in Fig. 1, but showing a zoom on the low-spin part of the level scheme.

via the $\alpha 3p$ reaction channel in the used reaction, and having a band with transitions of 411, 517, 622, 729, 797, 850, and 894 keV. The presence of the 997-keV transition is possibly due to the contamination from ^{116}Xe, a well populated nucleus via the $\alpha 2p$ reaction channel in the used reaction, and having the 524- and 616-keV transitions in the ground-state band, and the 998-keV transition in a Band 3 decaying to the ground-state band [13]. The absence of these transitions in the high-spin part of the positive-signature partner of Band 2 has important consequences: As will be discussed in the following section, it solves the problem of very different alignments in the signature partners of Band 2 reported in Ref. [4].

Band 3 has been identified starting from the 85- and 92-keV transitions previously reported in Ref. [4] and placed in parallel with the other transitions depopulating the $7/2^+$ state of Band 2, but only after inverting their order. The 85-keV transition is now a connecting transition between Band 2 to the new Band 3, while the 92-keV transition becomes the lowest dipole transition in Band 3, which is built on the $3/2^+$ ground state. Band 3 is composed of two rotational cascades of $E2$ transitions connected by $M1/E2$ transitions. Their spins and positive parity are fixed by the 92-keV $M1/E2$ [with a large mixing ratio of $-2.0(10)$] and 239-keV $E2$ transitions to the $3/2^+$ bandhead. Two out-of-band transitions have been identified towards states of Band 2. The connecting transitions in both directions between Bands 2 and 3 indicate strong mixing between the states with identical spin.

III. DISCUSSION

A. Alignment analysis

The quasiparticle alignments shown in Fig. 7 exhibit a large signature splitting between the signature partners of Band 1, and nearly degenerate signature partners in Bands 2 and 3.

The signature partners of the negative-parity Band 1 built on the $\nu h_{11/2}[541]3/2^-$ orbital exhibit alignments at a rotational frequency of $\hbar\omega \approx 0.35$ MeV. The alignment is due to $h_{11/2}$ protons, because the first $h_{11/2}$ neutron alignment predicted to occur at $\hbar\omega \approx 0.4$ MeV is blocked.

The aligned spin in the positive-parity Band 2 is higher by $\approx 1\hbar$ than that observed in Band 3 before the alignment, which occurs at similar rotational frequencies of $\hbar\omega \approx 0.35$ MeV in both bands. The alignment exhibits a back-bending in Band 3 and an up-bending in Band 2, suggesting a lower deformation of Band 3 relative to that of Band 2. As Bands 2 and 3 are assigned to the $\nu d_{5/2}[413]5/2^+$ and $\nu g_{7/2}[411]3/2^+$ configurations (see the following section), respectively, one would expect a higher alignment in Band 3, which is in contrast with the experimental alignment which is smaller than in Band 2. However, as the two configurations assigned to the Bands 2 and 3 are strongly mixed, the K values are difficult to define. An intermediate $K = 2$ value would lead to very similar alignments of the two bands. A second alignment is observed in Band 2 at $\hbar\omega \approx 0.46$ MeV, which was interpreted in Ref. [4] as due to $h_{11/2}$ neutrons. As the $\alpha = 1/2$ signature partner is populated up to a lower spin than the $\alpha = -1/2$ one, it is not clear if the alignment at $\hbar\omega \approx 0.46$ MeV is also present in the $\alpha = 1/2$ signature partner.

In Figs. 8 and 9 we have drawn the alignments observed in the negative-parity and positive-parity bands in the sequence of light odd-even Ba nuclei from ^{117}Ba and ^{123}Ba. One can see the evolution of the alignments in the negative-parity bands, where the alignment of the $-1/2$ signature partners are sharper than that of the $+1/2$ signature partners, and this sharpness increases with the neutron number. Only in the negative-parity signature of Band 1 in ^{123}Ba has a second alignment at $\hbar\omega \approx 0.6$ MeV been observed. For the positive-parity bands we had to change the spins by two and one units in ^{121}Ba and ^{123}Ba, respectively, to get a gradual change of the alignment with increasing neutron number, as suggested by calculations which show a gradual evolution of the structure along the chain of light Ba nuclei (see, e.g., Ref. [15]). One can observe similar alignment frequencies for all bands except for Bands 3 of ^{119}Ba and ^{121}Ba, in which the alignments are also sharper. In ^{119}Ba the negative-signature partner of Band 3 was observed after the second alignment up to high spin. In ^{117}Ba, the alignment of negative-signature partner of Band 2 is more gradual, and no second alignment was observed.

B. Particle number conserving cranked shell-model calculations

The possible configurations and alignment properties of the observed bands have been investigated through PNC-CSM calculations, in which the phenomenological Nilsson potential is adopted for the mean field [11], with parameters κ and μ taken from Ref. [16], and effective monopole paring strengths of 0.8 MeV for protons and 0.6 MeV for neutrons. This model was recently used to successfully describe the band structure in rare-earth nuclei [12]. In the present analysis we compared the calculated moments of inertia $J^{(1)}$ and the projection of the angular momentum J_x on the cranking axis with the experimental values. Single-quasiparticle neutron Routhian

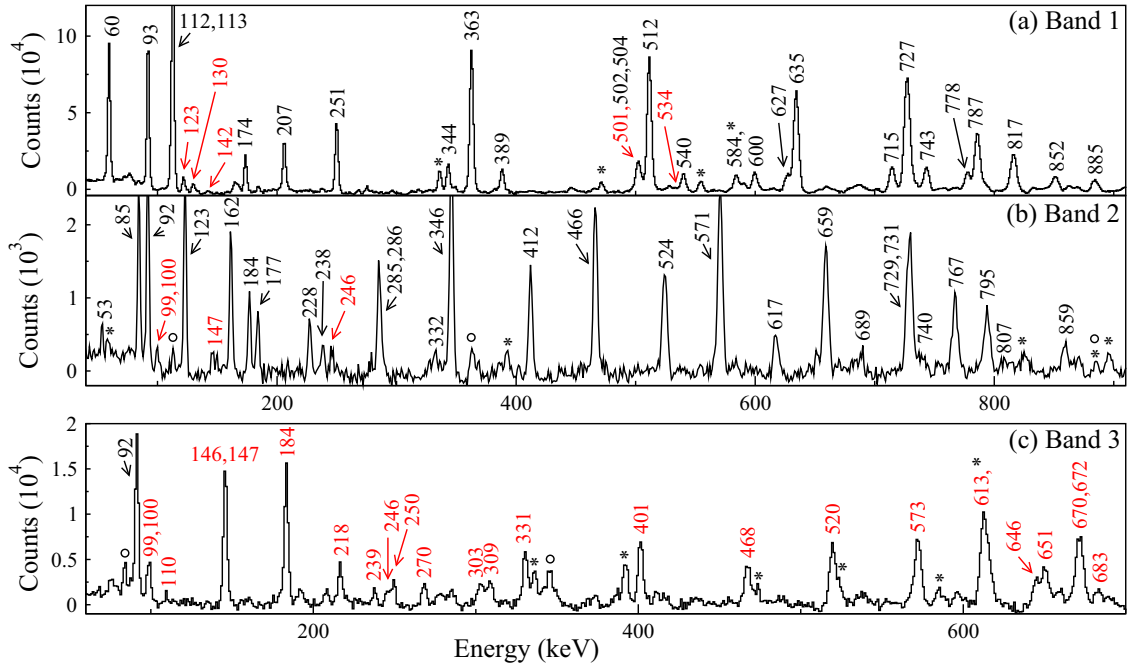

FIG. 3. Double-gated spectra showing the low- and medium-energy range for Bands 1, 2, and 3. Peak energies for the newly identified transitions are written in red. Transitions from ^{116}Xe, ^{118}Cs, ^{118}Xe, ^{119}Cs are indicated with an asterisk. while those of Band 1 of ^{118}Cs present in Band 2 are indicated with a circle. The spectra have been obtained as follows: The spectrum of Band 1 is the sum of the double-gated spectra obtained by gating on all combinations of the 93-, 113-, 207-, 344-, 363-, 502-, 512-, 627-, and 635-keV γ rays; the spectrum of Band 2 is the sum of the double-gated spectra obtained by gating on the 85- and 92-, 346- and 466-, 571- and 659-, and 617- and 689-keV γ rays; the spectrum of Band 3 is the sum of the double-gated spectra obtained by gating on all combinations of the 92-, 146-, 218-, 331-, 401-, 468-, 520-, and 651-keV γ rays.

diagrams as a function of rotational frequency for prolate and oblate deformations are shown in Fig. 10. They were used to guide the search of the closest quasiparticle orbitals to the proton and neutron Fermi surfaces.

The calculations were performed for an axial quadrupole deformation of $\varepsilon_2 = 0.32$, assumed to be equal to that resulting from the measured spectroscopic quadrupole moment of the neighboring ^{121}Ba nucleus [17,18], but higher by about 20% than those resulting from total Routhian surface (TRS) calculations ($\varepsilon_2 = 0.27$) [3–5].

To find the deformation which best describes Band 1, we calculated the assigned $\nu[532]5/2^-$ configuration for different deformations of $\varepsilon_2 = 0.29, 0.32, 0.35$ (see Fig. 11). The calculated moments of inertia for a deformation of $\varepsilon_2 = 0.32$ lead to good agreement for both signature partners. However, the alignments have a slightly different pattern in the two signature partners, being sharper and at lower rotational frequency in the $\alpha = 1/2$ partner. As one can see in Fig. 11, this can be induced by slightly different deformations, $\varepsilon_2 = 0.29$ for the $\alpha = 1/2$ partner and $\varepsilon_2 = 0.35$ for the $\alpha = -1/2$

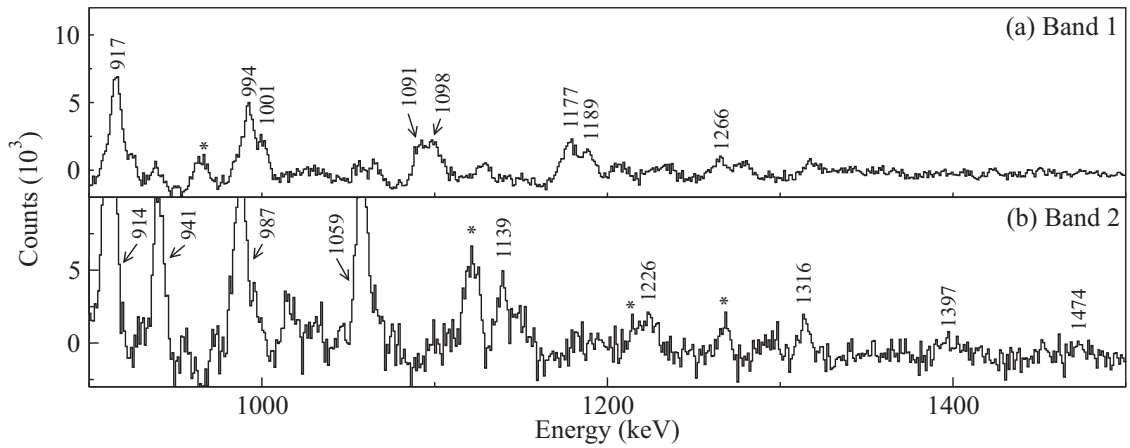

FIG. 4. The same as in Fig. 3 but showing the high-energy range for Bands 1 and 2.

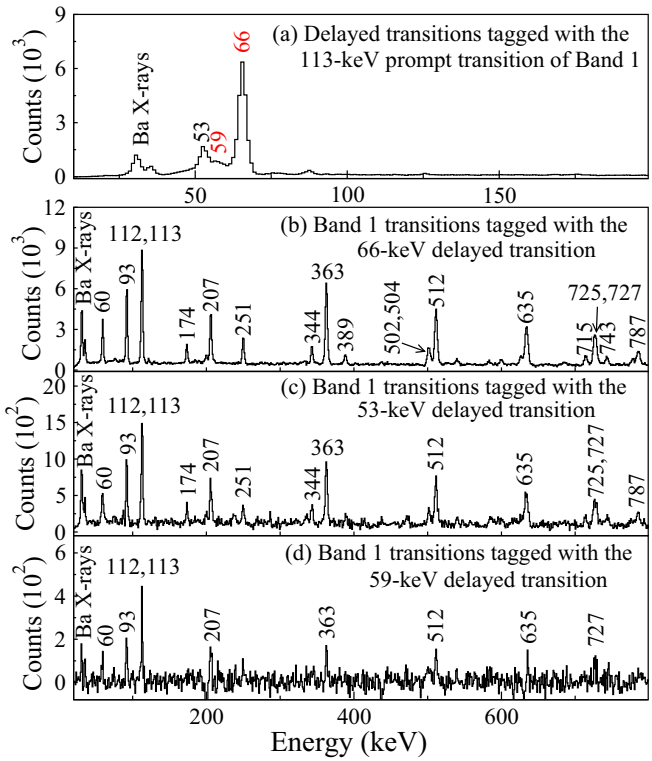

FIG. 5. Prompt-delayed coincidence spectra for Band 1. Peak energies for the newly identified transitions are written in red.

partner, as expected, because a higher deformation induces higher crossing frequency. The larger deformation induced by the $\alpha = -1/2$ signature partner is also expected, since its Routhian has a larger slope and therefore a larger deformation driving force (see Fig. 10). The frequency of the observed up-bending at $\hbar\omega \approx 0.4$ MeV is well reproduced by the calculations, being induced by the alignment of $h_{11/2}$ protons. A second level crossing is predicted for the $\alpha = 1/2$ partner at $\hbar\omega \approx 0.7$ MeV, which is induced by $h_{11/2}$ neutrons, but is beyond the observed frequency range of Band 1 and therefore

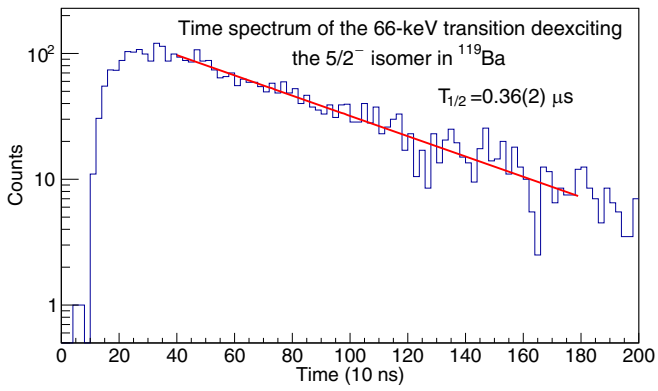

FIG. 6. Fit of the time spectrum of the delayed 66-keV transition deexciting the $5/2^-$ bandhead of Band 1 of ^{119}Ba, measured at the MARA focal plane, and produced by gating on the 93-, 113-, 207-, and 363-keV transitions detected with JUROGAM 3 at the target position.

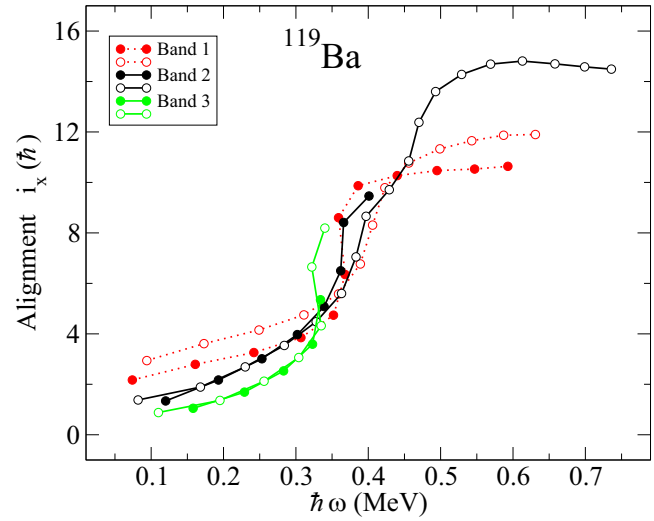

FIG. 7. Single-particle alignments i_x for the bands of ^{119}Ba. The Harris parameters are $J_0 = 17\,\hbar^2\,\mathrm{MeV}^{-1}$ and $J_0 = 25\,\hbar^4\,\mathrm{MeV}^{-3}$. The K values are 2.5, 2.5, and 1.5 for Bands 1, 2, and 3, respectively. The states with signature $\alpha = +1/2$ and $\alpha = -1/2$ are drawn with filled and open symbols, respectively. The positive-parity and negative-parity bands are drawn with continuous and dotted lines, respectively.

not confirmed. On the other hand, there is no second level crossing predicted for the $\alpha = -1/2$ partner.

Bands 2 and 3 are more difficult to reproduce by the present PNC-CSM calculations, mainly due to the mixing between the two bands at low rotational frequency. It has been previously recognized that the configuration of the known positive-parity bands in Ba nuclei changes from $\nu g_{7/2}[402]5/2^+$ in ^{123}Ba to $\nu d_{5/2}[413]5/2^+$ in ^{121}Ba, in agreement with spectroscopic quadrupole moments measurements [17,18]. The spectroscopic quadrupole moments of ^{117,119}Ba are not known experimentally. The $\nu d_{5/2}[413]5/2^+$ configuration assignment

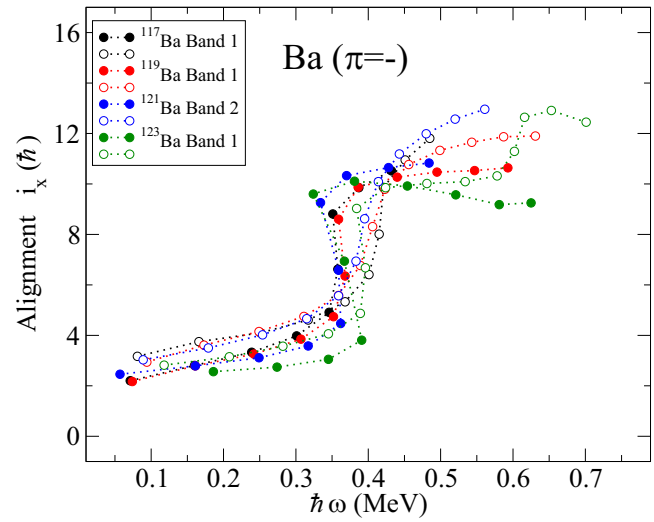

FIG. 8. The same as in Fig. 7 but for the negative-parity bands of ^{117,119,121,123}Ba. The K value is 2.5.

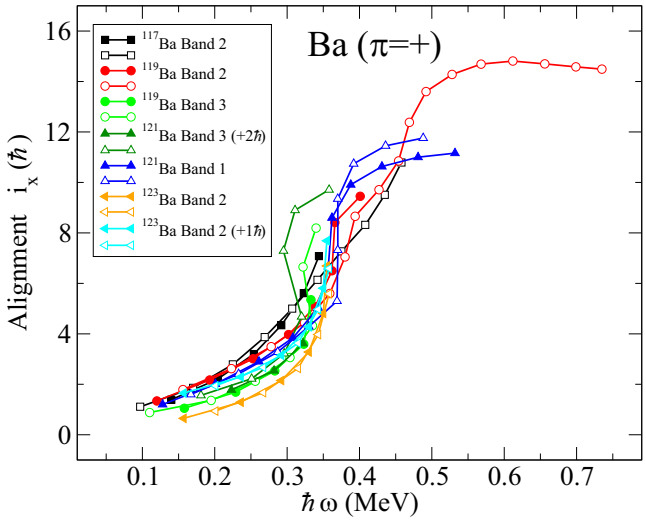

FIG. 9. The same as in Fig. 7 but for the positive-parity bands of ^{117,119,121,123}Ba. The K values are 1.5 for Bands 3 of ^{119,121}Ba, and 2.5 for the other bands.

was based on TRS and cranked shell-model calculations, which predict lower quadrupole deformations of $\varepsilon_2 = 0.27$. However, even with the higher adopted deformation in the present calculations $\varepsilon_2 = 0.32$, the $\nu d_{5/2}[413]5/2^+$ configuration assignment to the corresponding bands in ^{121,119}Ba remained unchanged, confirming the conclusion concerning the change of configuration from $\nu g_{7/2}[402]5/2^+$ in ^{123}Ba to $\nu d_{5/2}[413]5/2^+$ in the lighter ^{117,119,121}Ba nuclei. One can therefore exclude the $\nu[402]5/2^+$ configuration for Bands 2 and 3, because it is far away from the Fermi surface (see Fig. 10). The $\nu[411]1/2^+$ orbital is closer to the Fermi surface, but it has very large signature splitting, and therefore is inconsistent with the data. There remains only two positive-parity orbitals which are close to the Fermi surface and have small enough signature splitting in the low-frequency region

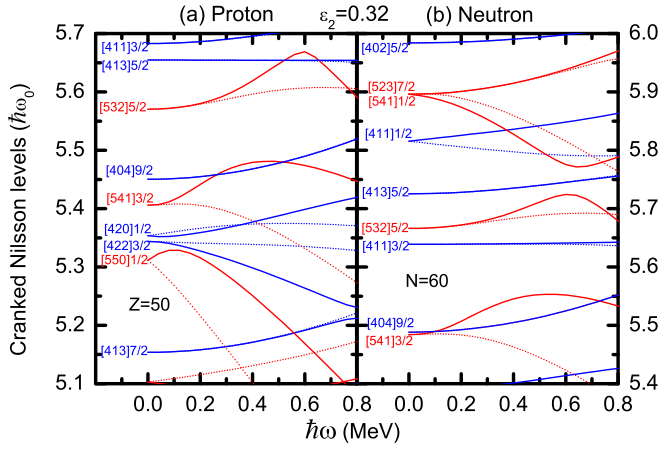

FIG. 10. Single-particle Routhians located in the vicinity of the Fermi level of ^{119}Ba as a function of rotational frequency for axial prolate deformation of $\varepsilon_2 = 0.32$: (a) protons and (b) neutrons. Positive (negative) parity Routhians are shown by blue (red) lines. Solid (dotted) lines are used for signature $\alpha = +1/2$ ($\alpha = +1/2$).

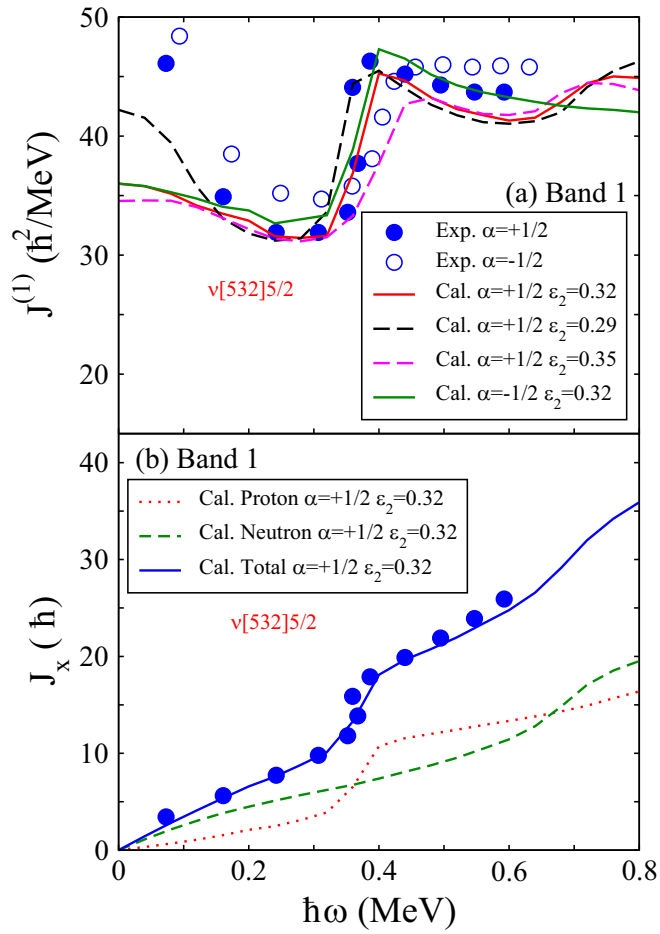

FIG. 11. (a) Moment of inertia $J^{(1)}$, experimental and calculated for three different deformations, (b) projection of the angular momentum on the cranking axis J_x for Band 1 of ^{119}Ba calculated using the PNC-CSM model for deformation $\varepsilon_2 = 0.32$. The states with signature $\alpha = +1/2$ and $\alpha = -1/2$ are drawn with filled and open symbols, respectively.

in agreement with the observed Bands 2 and 3: $\nu[411]3/2^+$ and $\nu[413]5/2^+$.

The two signature partners of Band 2 are quite similar up to the first up-bending observed at $\hbar\omega \approx 0.35$ MeV (see Fig. 7), which, based on the PNC-CSM calculations, is attributed to the $h_{11/2}$ protons. The $\alpha = 1/2$ signature partner, which is observed up to much higher spin than the $\alpha = -1/2$ one, exhibits a second alignment at $\hbar\omega \approx 0.45$ MeV. As one can see in Fig. 12, the frequency of the first up-bending induced by the $h_{11/2}$ protons is well reproduced, but the calculated $J^{(1)}$ is smaller than the experimental one. The frequency of the second alignment due to the $h_{11/2}$ neutrons is also well reproduced. However, the behavior of the $\alpha = -1/2$ partner of Band 2 above the second alignment is not well reproduced: Both the $J^{(1)}$ and J_x are smaller than the experimental values. The moment of inertia $J^{(1)}$ at low frequency is also overestimated by the present calculations. The calculated values can be changed by changing deformation, however, this will also lead to a change of the crossing frequency. In the present calculation, about a $7\hbar^2$/MeV change of $J^{(1)}$ is needed to

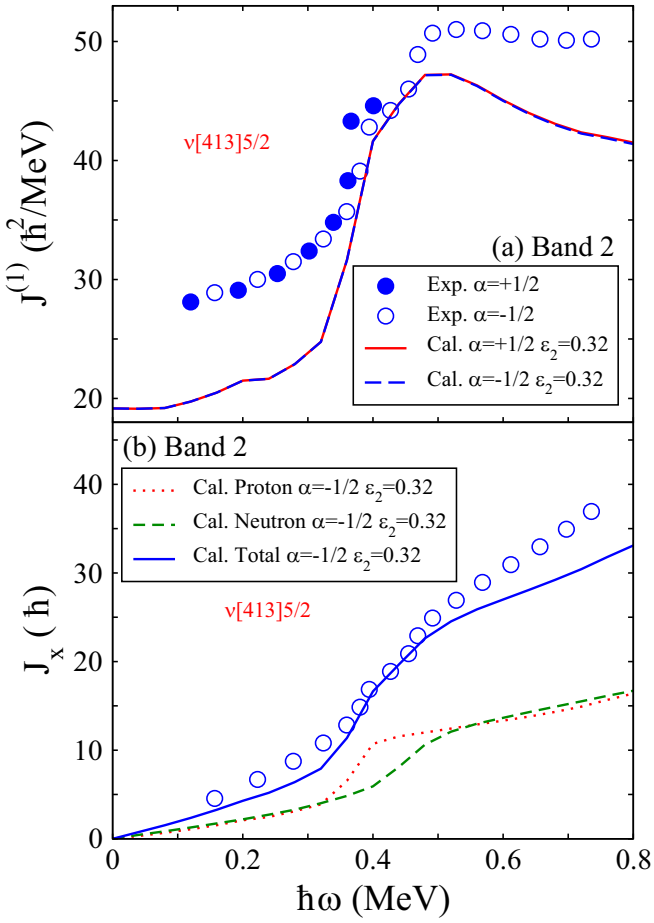

FIG. 12. The same as in Fig. 11 but for Band 2 of ^{119}Ba.

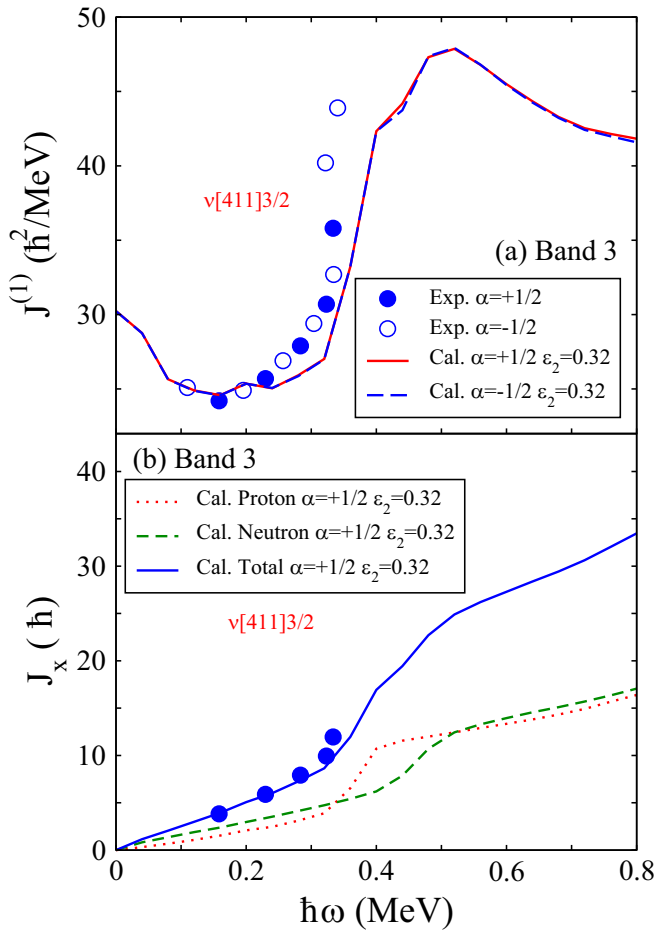

FIG. 13. The same as in Fig. 11 but for Band 3 of ^{119}Ba.

reproduce the experimental data. Such a change cannot be obtained by just changing the deformations and pairing strengths without changing the crossing frequency.

Band 3 is well reproduced by the $\nu[411]3/2^+$ configuration, except for the slightly higher calculated frequency of the up-bending induced by the alignment of the $h_{11/2}$ protons (see Fig. 13).

The nature of the $3/2^-$, 59-keV and $7/2^+$, 192-keV levels is not easy to establish.

IV. SUMMARY

The present work reports new results in ^{119}Ba, including one new band, several low-lying states, and the half-life measurement of the $5/2^-$ bandhead of the $\nu h_{11/2}$ band. The puzzle of the different alignment patterns in the previously known positive-parity band is solved. The observed bands enrich the knowledge of the neutron single-particle excitations in very proton-rich lanthanide nuclei. Configurations are assigned based on the analysis of the alignment properties and on PNC-CSM calculations, which are in good agreement with the experiment data and unveil the nature of the alignments observed in the different bands.

ACKNOWLEDGMENTS

This work has been supported by the China Scholarship Council (CSC), CSC No. 201804910386. This work has been supported by the Academy of Finland under the Finnish Centre of Excellence Programme (2012-2017), by the EU 7th Framework Programme Project No. 262010 (ENSAR), by the United Kingdom Science and Technology Facilities Council, by the National Research, Development and Innovation Fund of Hungary (Project No. K128947), as well as by the European Regional Development Fund (Contract No. GINOP-2.3.3-15-2016-00034); by the Polish National Science Centre (NCN) Grant No. 2013/10/M/ST2/00427; by the Swedish Research Council under Grant No. 2019-04880; and by the National Natural Science Foundation of China (Grants No. 11505242, No. 11305220, No. U1732139, No. 11775274, and No. 11575255). The use of germanium detectors from the GAMMAPOOL is acknowledged. I.K. was supported by National Research, Development and Innovation Office-NKFIH, Contract No. PD 124717.

APPENDIX

Table with experimental information on the γ-ray transitions of ^{119}Ba obtained in the present experiment.

TABLE I. Experimental information including the γ-ray energies E_γ, energies of the initial levels E_i, relative intensities I_γ, anisotropies $R_{\rm DCO}$ and/or $R_{\rm ac}$, parameters a_2 and a_4, polarization asymmetries A_p extracted following the prescription of Ref. [19], mixing ratios $\delta(M1/E2)$, multipolarities, and spin-parity assignments to the observed states in ^{119}Ba. The transitions listed with increasing energy are grouped in bands. The deduced values for $R_{\rm DCO}$ with a gate on stretched quadrupole transitions are ≈1 for stretched quadrupole and ≈0.46 for pure dipole transitions, while the ratio is close to 1 for a pure dipole and 2.1 for a stretched quadrupole transition when the gate is set on a pure dipole transition. The $R_{\rm ac}$ values for stretched dipole and quadrupole transitions are ≈0.8 and ≈1.4, respectively.

E_γ (keV)[a]	E_i (keV)	I_γ[b]	$R_{\rm DCO}$[c]	$R_{\rm ac}$[d]	a_2	a_4	A_p	δ	Mult.	$J_i^\pi \rightarrow J_f^\pi$
Band 1										
60.0	126.0	60(18)	1.0(1)[e]		−0.84(3)	0.46(5)		−1.8(4) or −0.3(4)	$M1/E2$	$(7/2^-) \rightarrow)5/2^-)$
92.5	332.2	104(8)	0.40(7)[f]		−0.70(4)	0.43(8)		−2.5(3) or −0.3(5)	$M1/E2$	$(11/2^-) \rightarrow (9/2^-)$
112.1	695.4	18(5)	0.41(5)[f]						$M1/E2$	$(15/2^-) \rightarrow (13/2^-)$
113.4	239.5	150(50)	0.53(6)[f]		−0.66(6)	0.37(5)		−2.6(6) or −0.2(4)	$M1/E2$	$(9/2^-) \rightarrow (7/2^{-)}$
122.6	1207.2	8(4)		0.9(2)					$M1/E2$	$(19/2^-) \rightarrow (17/2^-)$
130.2	1842.0	3(1)							$(M1/E2)$	$(23/2^-) \rightarrow (21/2^-)$
142.3	2568.9	2(1)							$(M1/E2)$	$(27/2^-) \rightarrow (25/2^-)$
174.0	239.5	30(10)	1.9(9)[e]		0.14(10)	−0.29(19)			$E2$	$(9/2^-) \rightarrow (5/2^-)$
206.5	332.2	100	0.93(7)[f]		0.29(3)	−0.19(5)	0.13(4)		$E2$	$(11/2^-) \rightarrow (7/2^-)$
250.5	583.0	50(10)	0.9(1)[e]		−0.68(8)	0.18(14)	−0.02(1)		$M1/E2$	$(13/2^-) \rightarrow (11/2^-)$
343.8	583.0	50(10)	2.2(3)[e]		0.33(5)	−0.02(7)	0.06(2)		$E2$	$(13/2^-) \rightarrow (9/2^-)$
363.2	695.4	250(50)	1.9(3)[e]		0.15(3)	−0.12(5)	0.08(2)		$E2$	$(15/2^-) \rightarrow (11/2^-)$
388.8	1084.5	30(10)		0.7(2)					$M1/E2$	$(17/2^-) \rightarrow (15/2^-)$
500.5	4673.1	6(4)							$(M1/E2)$	$(37/2^-) \rightarrow (35/2^-)$
501.7	1084.5	40(10)	0.95(9)[f]						$E2$	$(17/2^-) \rightarrow (13/2^-)$
504.1	1711.6	24(8)		0.7(2)					$M1/E2$	$(21/2^-) \rightarrow (19/2^-)$
511.8	1207.2	250(50)	1.0(1)[f]		0.11(9)	0.01(17)	0.14(4)		$E2$	$(19/2^-) \rightarrow (15/2^-)$
534.0	5558.1	3(1)							$(M1/E2)$	$(41/2^-) \rightarrow (39/2^-)$
539.8	3895.0	9(5)		0.9(1)					$M1/E2$	$(33/2^-) \rightarrow (31/2^-)$
584.0	2426.5	9(3)		0.5(3)					$M1/E2$	$(25/2^-) \rightarrow (23/2^-)$
600.4	3169.7	18(6)		0.6(2)					$M1/E2$	$(29/2^-) \rightarrow (27/2^-)$
627.2	1711.6	50(30)	1.1(2)[f]		0.03(14)	−0.07(26)			$E2$	$(21/2^-) \rightarrow (17/2^-)$
634.8	1842.0	180(40)	1.2(2)[f]		0.08(15)	0.10(27)	0.11(3)		$E2$	$(23/2^-) \rightarrow (19/2^-)$
715.0	2426.5	80(30)	1.3(2)[f]		0.02(14)	0.03(27)	0.08(4)		$E2$	$(25/2^-) \rightarrow (21/2^-)$
725.3	3895.0	40(20)		1.3(3)					$E2$	$(33/2^-) \rightarrow (29/2^-)$
726.9	2568.9	160(40)	1.0(2)[f]	1.3(1)	0.19(17)	−0.01(31)	0.13(4)		$E2$	$(27/2^-) \rightarrow ((23/2^-)$
743.4	3169.7	50(30)	1.0(2)[f]		0.06(19)	0.04(34)			$E2$	$(29/2^-) \rightarrow (25/2^-)$
778.1	4673.1	20(10)		1.5(3)					$E2$	$(37/2^-) \rightarrow (33/2^-)$
786.5	3355.4	83(20)	1.0(1)[f]						$E2$	$(31/2^-) \rightarrow (27/2^-)$
816.7	4172.1	50(10)	1.0(1)[f]						$E2$	$(35/2^-) \rightarrow (31/2^-)$
851.6	5023.7	24(7)	1.0(2)[f]						$E2$	$(39/2^-) \rightarrow (35/2^-)$
885.1	5558.1	20(10)		1.5(4)					$E2$	$(41/2^-) \rightarrow (37/2^-)$
916.6	5940.3	20(10)		1.3(2)					$E2$	$(43/2^-) \rightarrow (39/2^-)$
993.6	6551.7	19(10)		1.3(3)					$E2$	$(45/2^-) \rightarrow (41/2^-)$
1000.7	6941.0	9(3)		1.4(3)					$E2$	$(47/2^-) \rightarrow (43/2^-)$
1090.9	8031.9	6(3)		1.4(3)					$E2$	$(51/2^-) \rightarrow (47/2^-)$
1097.6	7649.3	10(6)		1.3(4)					$E2$	$(49/2^-) \rightarrow (45/2^-)$
1177.4	9209.3	6(2)		1.2(4)					$E2$	$(55/2^-) \rightarrow (51/2^-)$
1188.9	8838.2	8(5)		1.6(5)					$E2$	$(53/2^-) \rightarrow (49/2^-)$
1265.7	10475.0	4(2)							$(E2)$	$(59/2^-) \rightarrow (55/2^-)$
Band 1 → Ground state										
(7.4)	66.0								$(M1/E2)$	$(5/2^-) \rightarrow (3/2^-)$
58.6	58.6	10(4)							$(E1)$	$(3/2^-) \rightarrow (3/2^+)$
66.0	66.0	75(10)							$(E1)$	$(5/2^-) \rightarrow (3/2^+)$
Band 1 → Band 2										
(12.6)	66.0								$(E1)$	$(5/2^-) \rightarrow (5/2^+)$
Band 2										
123.1	176.5	45(9)	0.48(6)[f]		−0.91(17)	0.37(31)		−1.6(2) or −0.4(4)	$M1/E2$	$(7/2^{+)} \rightarrow (5/2^+)$
161.5	338.2	40(10)	1.2(1)[e]		−0.72(12)	0.40(23)	−0.14(5)	−2.3(2) or −0.3(5)	$M1/E2$	$(9/2^+) \rightarrow (7/2^+)$
183.9	522.3	30(10)	1.01(9)[e]		−0.69(12)	0.33(21)	−0.02(1)	−2.5(5) or −0.2(3)	$M1/E2$	$(11/2^+) \rightarrow (9/2^+)$
227.9	750.4	20(10)	0.53(9)[f]				−0.11(5)		$M1/E2$	$(13/2^+) \rightarrow (11/2^+)$

TABLE I. (*Continued.*)

E_γ (keV)[a]	E_i (keV)	I_γ[b]	$R_{\rm DCO}$[c]	$R_{\rm ac}$[d]	a_2	a_4	A_p	δ	Mult.	$J_i^\pi \rightarrow J_f^\pi$
238.2	988.7	11(5)		0.8(1)					$M1/E2$	$(15/2^+) \rightarrow (13/2^+)$
285.0	338.2	70(30)	0.94(9)[f]				0.13(5)		$E2$	$(9/2^+) \rightarrow (5/2^+)$
285.5	1559.4	4(3)							$(M1/E2)$	$(19/2^+) \rightarrow (17/2^+)$
285.9	1274.7	5(4)							$(M1/E2)$	$(17/2^+) \rightarrow (15/2^+)$
332.2	1892.1	3(3)							$(M1/E2)$	$(21/2^+) \rightarrow (19/2^+)$
345.8	522.3	110(40)	0.86(7)[f]		0.15(3)	−0.25(5)	0.06(2)		$E2$	$(11/2^+) \rightarrow (7/2^+)$
412.2	750.4	110(40)	0.94(9)[f]		0.15(10)	−0.32(18)	0.15(8)		$E2$	$(13/2^+) \rightarrow (9/2^+)$
466.4	988.7	120(40)	1.01(6)[f]		−0.06(15)	−0.30(28)	0.06(2)		$E2$	$(15/2^+) \rightarrow (11/2^+)$
524.3	1274.7	100(50)	1.18(9)[f]		−0.03(7)	−0.17(12)	0.15(7)		$E2$	$(17/2^+) \rightarrow (13/2^+)$
570.7	1559.4	100(40)	1.0(1)[f]		0.15(10)	−0.01(10)	0.09(4)		$E2$	$(19/2^+) \rightarrow (15/2^+)$
617.4	1892.1	80(40)		1.3(2)	0.22(8)	0.02(14)	0.11(6)		$E2$	$(21/2^+) \rightarrow (17/2^+)$
659.2	2218.6	80(40)	1.2(2)[f]		0.24(16)	0.06(29)	0.18(9)		$E2$	$(23/2^+) \rightarrow (19/2^+)$
688.7	2580.8	60(30)		1.3(2)	0.11(27)	−0.02(49)	0.11(9)		$E2$	$(25/2^+) \rightarrow (21/2^+)$
728.7	2947.3	60(30)	1.3(3)[f]						$E2$	$(27/2^+) \rightarrow (23/2^+)$
731.4	3312.2	45(20)	1.1(3)[f]						$E2$	$(29/2^+) \rightarrow (25/2^+)$
767.2	3714.5	35(20)		1.6(5)					$E2$	$(31/2^+) \rightarrow (27/2^+)$
740.0	4052.2	15(8)		1.4(4)					$E2$	$(33/2^+) \rightarrow (29/2^+)$
794.8	4509.3	35(20)		1.6(4)					$E2$	$(35/2^+) \rightarrow (31/2^+)$
807.0	4859.2	8(4)		1.2(5)					$E2$	$(37/2^+) \rightarrow (33/2^+)$
859.1	5368.4	16(9)		1.3(2)					$E2$	$(39/2^+) \rightarrow (35/2^+)$
913.9	6282.3	11(7)		1.5(5)					$E2$	$(43/2^+) \rightarrow (39/2^+)$
941.3	7223.6	10(7)		1.4(6)					$E2$	$(47/2^+) \rightarrow (43/2^+)$
987.0	8210.6	9(5)		1.4(3)					$E2$	$(51/2^+) \rightarrow (47/2^+)$
1059.3	9269.9	7(4)		1.3(4)					$E2$	$(55/2^+) \rightarrow (51/2^+)$
1139.4	10409.3	4(2)							$E2$	$(59/2^+) \rightarrow (55/2^+)$
1225.6	11634.9	2(1)							$E2$	$(63/2^+) \rightarrow (59/2^+)$
1315.8	12950.7	1(1)							$E2$	$(67/2^+) \rightarrow (63/2^+)$
1397.0	14347.7	<1							$E2$	$(71/2^+) \rightarrow (67/2^+)$
1473.9	15821.6	<1							$E2$	$(75/2^+) \rightarrow (71/2^+)$
Band 2 → Band 3										
53.3	53.3	20(10)		0.7(1)					$M1/E2$	$(5/2^+) \rightarrow (3/2^+)$
84.5	176.5	32(6)	0.5(1)[f]		−0.73(13)	0.64(25)		−2.2(9) or −0.2(4)	$M1/E2$	$(7/2^+) \rightarrow (5/2^+)$
99.2	988.7	3(2)							$(M1/E2)$	$(15/2^+) \rightarrow (13/2^+)$
99.3	522.3	5(4)							$(M1/E2)$	$(11/2^+) \rightarrow (9/2^+)$
109.9	750.4	4(2)							$(M1/E2)$	$(13/2^+) \rightarrow (11/2^+)$
177.0	176.5	17(3)		1.2(3)					$E2$	$(7/2^+) \rightarrow (3/2^+)$
246.3	338.2	16(7)		1.4(4)					$E2$	$(9/2^+) \rightarrow (5/2^+)$
Band 2 → $7/2^+$										
146.5	338.2	12(5)		0.9(2)					$M1/E2$	$(9/2^+) \rightarrow (7/2^+)$
$7/2^+$ → Band 3										
99.6	191.5	12(5)		0.5(2)					$M1/E2$	$(7/2^+) \rightarrow (5/2^+)$
Band 3										
91.9	91.9	120(60)	0.5(1)[f]		−0.73(15)	0.66(27)		−2.0(10) or −0.2(5)	$M1/E2$	$(5/2^+) \rightarrow (3/2^+)$
146.3	238.4	56(20)	0.5(1)[f]		−0.72(4)	0.32(6)	−0.02(1)	−2.2(8) or −0.2(3)	$M1/E2$	$(7/2^+) \rightarrow (5/2^+)$
184.2	422.6	34(8)	1.3(3)[e]		−0.47(5)	0.46(6)	−0.16(9)	−3.8(6) or −0.1(5)	$M1/E2$	$(9/2^+) \rightarrow (7/2^+)$
217.5	639.9	18(7)		0.8(2)					$M1/E2$	$(11/2^+) \rightarrow (9/2^+)$
238.9	238.4	17(9)	1.0(2)[f]						$E2$	$(7/2^+) \rightarrow (3/2^+)$
249.8	890.2	9(4)		1.0(4)					$M1/E2$	$(13/2^+) \rightarrow (11/2^+)$
269.6	1159.8	7(4)							$(M1/E2)$	$(15/2^+) \rightarrow (13/2^+)$
302.5	1462.7	4(2)							$(M1/E2)$	$(17/2^+) \rightarrow (15/2^+)$
309.1	1772.3	<2							$(M1/E2)$	$(19/2^+) \rightarrow (17/2^+)$
330.8	422.6	31(6)	2.1(4)[e]		−0.08(28)	−0.22(53)			$E2$	$(9/2^+) \rightarrow (5/2^+)$
401.4	639.9	50(13)	2.0(4)[e]		−0.07(23)	−0.33(43)	0.02(1)		$E2$	$(11/2^+) \rightarrow 7(/2^+)$
467.7	890.2	50(20)	1.7(3)[e]		0.02(21)	0.02(40)	0.04(2)		$E2$	$(13/2^+) \rightarrow (9/2^+)$
520.0	1159.8	50(30)	0.9(3)[f]		0.02(31)	0.05(58)	0.09(4)		$E2$	$(15/2^+) \rightarrow (11/2^+)$
572.6	1462.7	30(15)		1.2(3)	0.16(28)	0.21(52)			$E2$	$(17/2^+) \rightarrow (13/2^+)$
612.5	1772.3	47(20)	1.2(2)[f]		0.25(30)	0.35(55)	0.02(2)		$E2$	$(19/2^+) \rightarrow (15/2^+)$
645.8	3090.4	11(5)		1.3(3)					$E2$	$(27/2^+) \rightarrow (23/2^+)$

TABLE I. (*Continued.*)

E_γ (keV)[a]	E_i (keV)	I_γ[b]	R_{DCO}[c]	R_{ac}[d]	a_2	a_4	A_p	δ	Mult.	$J_i^\pi \rightarrow J_f^\pi$
650.8	2113.5	20(10)		1.4(3)					$E2$	$(21/2^+) \rightarrow (17/2^+)$
670.2	2783.7	12(6)		1.6(5)					$E2$	$(25/2^+) \rightarrow (21/2^+)$
672.3	2444.6	40(18)	1.0(2)[f]	1.4(2)					$E2$	$(23/2^+) \rightarrow (19/2^+)$
683.0	3773.4	7(3)		1.3(5)					$E2$	$(31/2^+) \rightarrow (27/2^+)$
Band 3 → Band 2										
245.9	422.6	6(3)							$(M1/E2)$	$(9/2^+) \rightarrow (7/2^+)$
302.2	639.9	5(2)							$(M1/E2)$	$(11/2^+) \rightarrow (9/2^+)$

[a]The error on the transition energies is 0.3 keV for transitions below 500 keV, 0.7 keV for transitions between 500 and 1000 keV, and 1.0 keV for transitions above 1000 keV. The error on the transition transition energies is 1.0 keV for the transition intensities less than 5.
[b]Relative intensities corrected for efficiency, normalized to the intensity of the 206.5 keV, $11/2^- \rightarrow 7/2^-$ transition of Band 1. The transition intensities were obtained from a combination of total projection and gated spectra.
[c]R_{DCO} has been deduced from an asymmetric γ-γ coincidence matrix sorted with the detectors at 157.6° on one axis, and the detectors at ≈90° on the other axis. The tentative spin-parity of the states are given in parentheses.
[d]R_{ac} has been deduced from two asymmetric γ-γ coincidence matrices sorted with the detectors at 133.6157.6° on one axis, and the detectors at ≈90° on the other axis. The tentative spin-parity of the states are given in parentheses.
[e]DCO ratio from spectrum gated on stretched dipole transition.
[f]DCO ratio from spectrum gated on stretched quadrupole transition.

[1] I. Y. Lee, Nucl. Phys. A **520**, c641 (1990).
[2] N. Davids and D. Larson, Nucl. Instrum. Methods Phys. Res., Sect. B **40-41**, 1224 (1989).
[3] B. Ding *et al.*, Phys. Rev. C **95**, 024301 (2017).
[4] J. F. Smith *et al.*, Phys. Rev. C **61**, 044329 (2000).
[5] B. Cederwall *et al.*, Nucl. Phys. A **529**, 410 (1991).
[6] J. Pakarinen *et al.*, Eur. Phys. J. A **56**, 149 (2020).
[7] J. Sarén *et al.*, Nucl. Instrum. Methods Phys. Res., Sect. B **266**, 4196 (2008).
[8] K. K. Zheng *et al.*, Chiral bands in ^{119}Cs, Phys. Lett. B (to be published).
[9] K. K. Zheng *et al.*, Oblate-prolate coexistence in ^{119}Cs, Phys. Lett. B (to be published).
[10] K. K. Zheng *et al.*, Complete spectroscopy in ^{119}Cs, Phys. Rev. C (to be published).
[11] J. Y. Zeng, T. H. Jin, and Z. J. Zhao, Phys. Rev. C **50**, 1388 (1994).
[12] Z. H. Zhang, M. Huang, and A. V. Afanasjev, Phys. Rev. C **101**, 054303 (2020).
[13] ENSDF, NNDC Online Data Service, ENSDF database, http://www.nndc.bnl.gov/ensdf/.
[14] D. D. Bogdanov, A. V. Demyanov, V. A. Karnaukhov, L. A. Petrov, and J. Voboril, Nucl. Phys. A **303**, 145 (1978).
[15] N. A. Smirnova, B. Blank, B. A. Brown, W. A. Richter, N. Benouaret, Y. H. Lam, Phys. Rev. C **95**, 054301 (2017).
[16] T. Bengtsson and I. Ragnarsson, Nucl. Phys. A **436**, 14 (1985).
[17] S. A. Wells *et al.*, Phys. Lett. B **211**, 272 (1988).
[18] A. C. Mueller, F. Buchinger, W. Klempt, E. W. Otten, R. Neugart, C. Ekström, and J. Heinemeier, Nucl. Phys. A **403**, 234 (1983).
[19] K. Starosta *et al.*, Nucl. Instrum. Methods Phys. Res., Sect. A **423**, 16 (1999).